Optical properties of Cu^+ ions in $RbMgF_3$ crystals

K. Tanimura and W. A. Sibley
Physics Department, Oklahoma State University, Stillwater, Oklahoma 74078

L. G. DeShazer
Hughes Research Laboratory, Malibu, California 90265

(Received 24 August 1984)

The absorption, emission, and excitation spectra, as well as the lifetimes, have been measured for Cu^+ ions substituting for Rb^+ ions in two different sites in $RbMgF_3$ crystals. The $(3d)^{10} \rightarrow (3d)^9(4s)$ absorption transitions occur in the ultraviolet with optical emission at 450 and 575 nm. The two emission bands have been attributed to Cu^+ ions occupying two different sites. From the results of polarized excitation experiments, the electronic structure of the crystal-field-split levels of the $(3d)^9(4s)$ configuration of Cu^+ ions at the two sites can be determined. The 575-nm luminescence is quenched above 300 K. This quenching is ascribed to nonradiative multiphonon emission which is enhanced significantly by strong nonlinear electron-phonon coupling.

I. INTRODUCTION

The need for tunable lasers has accentuated the necessity for an understanding of the optical properties of impurities situated in host materials which exhibit optical transmission from 200 nm to 10 μm. One such impurity is the Cu^+ ion, which has a $(3d)^{10}$ electronic configuration in the ground state. This ion has been studied in a number of simple alkali-halide hosts.[1–16] These investigations have increased our understanding of the interconfigurational transitions ($d \rightarrow s$ and $d \rightarrow p$) of metal ions in solids, and the effect of off-center defect configurations on the ground and excited states. From these studies the following properties of Cu^+ ions have been determined. When Cu^+ ions substitute for the host cation with larger ionic radius, they occupy off-center sites in the ground state. The $3d \rightarrow 4s$ transition energy of Cu^+ is almost independent of host crystal. The luminescence of Cu^+ ions arises from transitions between the lowest triplet level of the $(3d)^9(4s)$ configuration and the $(3d)^{10}$ ground state, and, finally, the lifetime of the luminescence shows a strong temperature dependence which is attributed to the thermal population of the spin-orbit-split lowest excited-state level.

The optical emission from Cu^+ ions in $RbMgF_3$ was observed previously.[17] The observed spectroscopic characteristics of Cu^+ ions in this material is considerably different from those of the simple alkali halides. The purpose of this investigation is to use detailed spectroscopic data to form a complete picture of the optical properties of Cu^+ ions in $RbMgF_3$ crystals. These crystals have the hexagonal $BaTiO_3$ crystal structure. In this lattice the Cu^+ ions substitute for Rb^+ ions which reside at two different sites in the lattice. One site symmetry is C_{3v} and the other D_{3h}. Since the crystal is optically anisotropic, polarization measurements yield valuable information about the nature of the excited states for Cu^+ ions in two different site symmetries.

II. EXPERIMENTAL PROCEDURES

The growth of $RbMgF_3$ by the Czochralski method, utilizing a dry HF atmosphere, produces transparent crystals with minimum OH^- concentration. In order to reduce the OH^- concentration reactive atmosphere processing is used. In the past this has been found to be highly effective in removing OH^- from many types of materials.[18–20] In the growth process the furnace is loaded with a vitreous carbon crucible containing $RbMgF_3$, which has been prepared by sintering at 500 °C in a fluorine atmosphere. When copper-doped $RbMgF_3$ is desired, copper metal is added to the crucible to establish an equilibrium between Cu^{1+} and Cu^0 which maximizes the Cu^{1+} doping level. The furnace is evacuated to 10^{-3} torr at room temperature and then filled with two atmospheres of helium which is slowly released at a constant flow of 3 l/min. An HF flow of 0.2 l/min is initiated and maintained throughout the run. The temperature of the charge is raised to 900 °C in 4 h at which time a CF_4 flow of 0.1 l/min is initiated and maintained. The pull rate is about 4 mm/h and the pull rod rotation speed is 15 rpm. Since the Cu^{1+} substitutes for Rb^+ and the ionic radii are almost a factor of 2 different, substitutional doping is difficult and very little copper enters the $RbMgF_3$ crystal. Even though 2% copper was in the melt an EDAX analysis indicated that the concentration of Cu^+ in the crystal was only a few ppm.

Optical-absorption measurements were made with a Perkin Elmer 330 spectrophotometer. Emission and excitation spectra were taken by exciting the samples with light from a 300-W xenon-arc lamp passed through a 0.22-m Spex monochromator. The fluorescence was focused into a 1.0-m Jarrell-Ash monochromator and a mirror was used to route the light emerging from the exit slit to the appropriate detector. The detector in this case was a cooled RCA Model No. C31034 photomultiplier tube. The intensity of the excited light was calibrated

utilizing a Rhodamine B quantum counter. The emission monochromator and photomultiplier tube response were corrected using a quartz-iodine lamp traceable to the National Bureau of Standards. The detector signal was preamplified and passed to a lock-in amplifier that was synchronized with a variable-speed light chopper in the excitation beam. The output of the lock-in amplifier may be displayed on an X-Y recorder or stored by a Hewlett-Packard Model No. HP-85 minicomputer.

Lifetime measurements were made by utilizing a Biomation 610B transient recorder and a Nicolet 1070 signal averager. This system allowed lifetimes as short as 10 μs to be measured. Lifetimes shorter than 10 μs were measured using a Molectron UV14 nitrogen laser and a Princeton Applied Research 162 boxcar integrator in the laboratory of R. C. Powell. This system can measure lifetimes as short as 20 ns.

For low-temperature measurements a CTI Cryodyne Cryocooler Model No. 21SC was utilized. High-temperature measurements were made with the sample enclosed in a copper holder with small windows for the excitation and emission light. Temperature control was accomplished using resistance heaters. Temperature control below room temperature was ± 1 K, while above room temperature it was ± 5 K.

III. EXPERIMENTAL RESULTS

A. Overview of results

Figure 1 illustrates the optical-absorption spectrum for an unoriented $RbMgF_3$:Cu^+ sample measured at 300 K. The base line of the absorption curve was carefully subtracted by comparing the absorption with that for pure $RbMgF_3$. Two distinct peaks are observed; one at 209 nm (47 900 cm^{-1}) and another, with structure, at about 295 nm (33 900 cm^{-1}). The vertical lines in the figure indicate the peak energies of the optical absorption of Cu^+ ions in several alkali-halide hosts.[1,3,8,14,15] The peak energy similarities between those reported for alkali halides and the low-energy band in $RbMgF_3$:Cu^+ strongly suggests that the 295-nm absorption band is due to the $(3d)^{10} \rightarrow (3d)^9(4s)$ transition of Cu^+ ions. The origin of

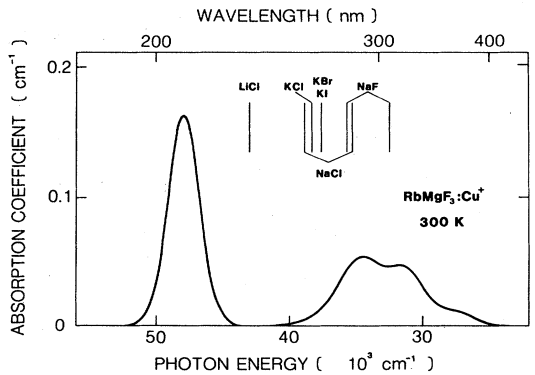

FIG. 1. Optical absorption of $RbMgF_3$:Cu^+ at 300 K. The lines in the figure indicate reported Cu^+-ion absorption in various alkali-halide crystals.

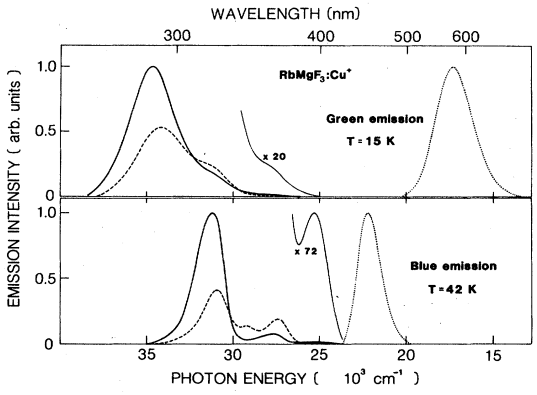

FIG. 2. Luminescence from $RbMgF_3$:Cu^+ crystals at 15 and 42 K when excited with 300-nm light (dotted curves). Solid and dashed curves on the left-hand side of the figure portray the excitation spectra for the blue and green emission, measured with the electric vector parallel and perpendicular to the c axis, respectively.

the absorption band at 209 nm (47 850 cm^{-1}) is not certain at this time. When the $3d \rightarrow 4s$ transition band shown in Fig. 1 at 295 nm is excited in an oriented crystal, two emission bands appear. One band occurs at 450 nm (22 300 cm^{-1}) and the other at 575 nm (17 300 cm^{-1}). This is illustrated by the dotted lines on the right-hand side of Fig. 2. Both of these bands are partially polarized with the electric vector of the emitted light along the c axis of the crystal. Excitation spectra can provide more definitive information than optical absorption. Therefore, extensive excitation spectra measurements were made from the Cu^+ luminescence portrayed in Fig. 2. These detailed emission and excitation spectra provide specific information on the electronic structure of the *higher-energy states of Cu^+ ions*. The left-hand side of Fig. 2 portrays the excitation spectra for the 450- and 575-nm emission bands measured with the electric vector ($\mathbf{E}$) both parallel ($\mathbf{E} \| \hat{\mathbf{c}}$), solid line, and perpendicular ($\mathbf{E} \perp \hat{\mathbf{c}}$), dashed line, to the $\mathbf{c}$ axis. It should be noted that the sum of the excitation spectra in the figure is quite similar to the absorption band at 295 nm in Fig. 1. Even though peak energies and widths of the excitation spectra are different for the two emission bands, there are similarities. The most intense excitation peaks are polarized $\mathbf{E} \| \hat{\mathbf{c}}$, and appear at the highest-energy region. The spectra of the $\mathbf{E} \perp \hat{\mathbf{c}}$ excitation components show two dominant bands with a splitting of 3500 cm^{-1}. For the 450-nm emission, the lowest-energy *excitation* peak has mirror symmetry with the *emission* band. The lowest excitation band for the 575-nm emission is situated at about 364 nm (27 500 cm^{-1}). These similarities suggest that the centers responsible for the two luminescence bands are Cu^+ ions situated in different environments. If so, there should be an intensity correlation if the ions can move from one site to another. Isochronal pulse annealing experiments (samples held 15 min at a fixed temperature, quenched to 300 K, and then measured) were performed to confirm this. Figure 3 shows the changes in luminescence intensity, as a

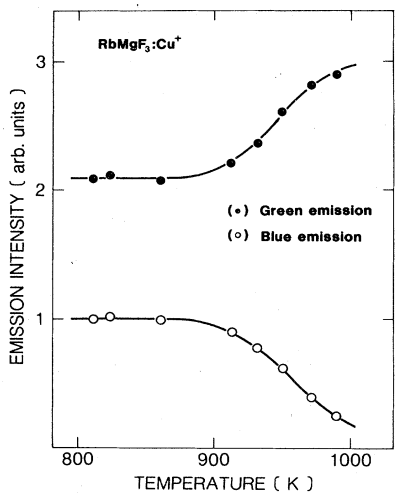

FIG. 3. Blue and green emission intensity as a function of annealing temperature.

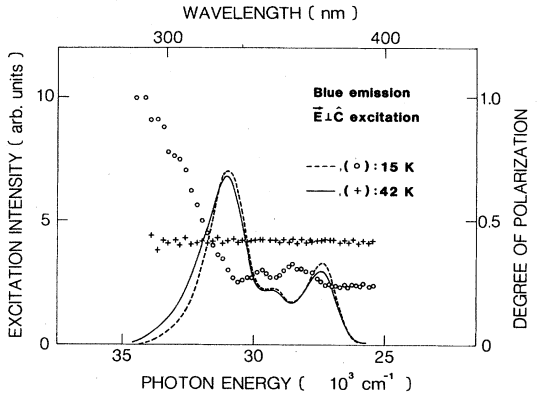

FIG. 4. Excitation spectra for the $\mathbf{E}\|\hat{c}$ component of the 450-nm emission at 15 and 42 K with the exciting light polarized $\mathbf{E}\perp\hat{c}$. The degree of polarization of the 450-nm band is also shown as a function of excitation photon energy. The circles show the degree of polarization as a function of excitation energy at 15 K and the pluses are for data taken at 42 K.

function of annealing temperature. The intensity of the 450-nm emission (open circles) decreases, whereas that of the 575-nm emission (solid circles) increases with temperature above 850 K. The data, shown in the figure, clearly suggest that the centers responsible for the 450- and 575-nm emissions are Cu^+ ions in different configurations or environments. The concentration change could not be reversed even though various cooling rates from 100 deg/min to 0.1 deg/min were used. This observation suggests that Cu^+ aggregates or pairs are not responsible for the emission since the concentration of aggregated ions should change markedly with cooling rate.

It was noted in the Introduction that two distinct Rb^+ sites are present in $RbMgF_3$. There are twice as many sites of one kind than the other. If the relative concentration of Cu^+ ions responsible for the two absorption or excitation spectra around 295 nm can be determined, then the sites responsible for the bands can be assigned. The integrated area of excitation spectra for the respective emissions is defined as

$$I=\sum_p \int S_p(\nu)d\nu \ . \tag{1}$$

In the equation $S_p(\nu)$ is the integrated area of an emission band excited by light having a frequency ν and polarization p. The integrated intensity I is proportional to the concentration N and the oscillator strength f of the Cu^+-ion transitions. At 48 K the ratio of I for the 575-nm emission to that for the 450-nm emission is found to be 2. If it is assumed that the summed oscillator strengths of transitions in energy region from 24 000 to 42 000 cm^{-1} are the same for both centers, then the results indicate that the concentration of the center responsible for the 575-nm emission is twice that of those responsible for the 450-nm emission. These data can be used to help develop an energy-level diagram for Cu^+ ions. In the following subsections detailed data for each center are presented for use in both site assignment and energy-level determinations.

B. The 450-nm "blue" emission

The excitation spectra for the $\mathbf{E}\|\hat{c}$ component of the 450-nm emission taken at 15 and 42 K with the exciting light polarized $\mathbf{E}\perp\hat{c}$ are shown in Fig. 4. The 323-nm (31 000 cm^{-1}) peak appears to "narrow" with increasing temperature. Similar narrowing was found for the $\mathbf{E}\|\hat{c}$ excitation spectra. Figure 4 also includes the degree of polarization $P=(I_{\|}-I_{\perp})/(I_{\|}+I_{\perp})$ of the 450-nm emission as a function of excitation energy, where $I_{\|}$ and $I_{\perp}$ represent the emission intensities, the electric vectors of which are parallel and perpendicular to the c axis. At 15 K the degree of polarization of the emission depends strongly on the excitation energy. Luminescence excited by energies higher than 305 nm (33 000 cm^{-1}) is polarized along the c axis, whereas excitation at energies lower than 370 nm (27 000 cm^{-1}) is only weakly polarized. On the other hand, the degree of polarization becomes constant at 42 K and higher temperatures for all excitation-photon energies.

The emission spectra at 450 nm excited by 305- and

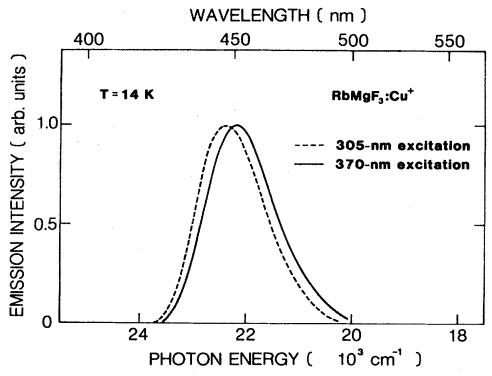

FIG. 5. Emission spectra at 14 K from $RbMgF_3:Cu^+$ excited with 305- and 370-nm light.

370-nm light are shown in Fig. 5. The intensities are normalized to unity at the maxima. The band excited by 305-nm light has a higher peak energy by 200 cm^{-1} than that due to 370-nm excitation. The former emission band is almost completely polarized $\mathbf{E}||\hat{c}$, whereas the latter is partially polarized along the same direction.

These results show that at 15 K two sets of excitation peaks exist for two different "blue" luminescence bands. Since one luminescence band is completely polarized along the c axis, the excitation spectra for the $\mathbf{E}\perp\hat{c}$ component of the luminescence do not include any peaks for this completely-polarized luminescence, and the excitation spectra can be deconvoluted. The result of such an analysis is shown in Fig. 6 for excitation spectra with the incident light polarized (a) $\mathbf{E}||\hat{c}$ and (b) $\mathbf{E}\perp\hat{c}$. The solid curve in Fig. 6 is the excitation spectra for the slightly-polarized emission band (450 nm). The dashed curve represents the excitation spectra of the completely-polarized emission band at 446.4 nm. The ratio of the integrated excitation band intensities was found to be 0.18. Apparently at low temperatures the Cu^+ ions in this site have two different configurations and give rise to two similar, but different spectra.

From the temperature-dependent changes of the emission intensities excited by 305- and 370-nm light, it appears that around 30 K the center responsible for the 446.4-nm emission converts to the center responsible for the 450-nm emission. Above 40 K only one type of configuration, which gives rise to the 450-nm emission, exists. Detailed measurements were made on the 450-nm emission. For measurements below 40 K, wavelength and polarization of exciting light was properly chosen so that only the 450-nm emission was excited. The lifetime and the integrated intensity of the 450-nm emission as a function of temperature is illustrated in Fig. 7. The rapid decrease and saturation of the lifetime (without any loss of luminescence intensity) is characteristic of the thermalization of two energy levels separated only slightly in energy but with different oscillator strengths. When zero-phonon lines are present in absorption or emission spectra, it is at times possible to distinguish both levels at low temperature. Figure 8 shows the fine structure of the 450-nm emission excited by 370-nm light. The $\mathbf{E}\perp\hat{c}$ emission shows lines at 23 603, 23 507, and 23 410 cm^{-1}. The separation of the three lines is 95 cm^{-1}. On the other hand, the $\mathbf{E}||\hat{c}$ emission spectrum shows a polarized line at 23 656 cm^{-1}. The partial c-axis polarization of the broad band is ascribed to the superposition of the two components. The separation of the levels responsible for these components is 53 cm^{-1}. At higher temperature, the degree of polarization of the 450-nm broadband was found to increase with increasing temperature. It is 0.40 at 40 K, 0.50, at 60 K, and 0.63 at 200 K. The increase in the degree of polarization is attributed to the thermaliza-

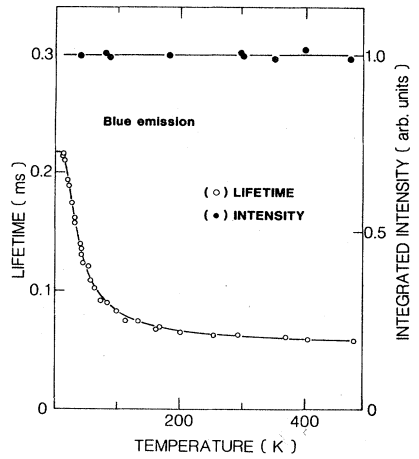

FIG. 7. Lifetime and integrated emission intensity as a function of temperature for the 450-nm emission.

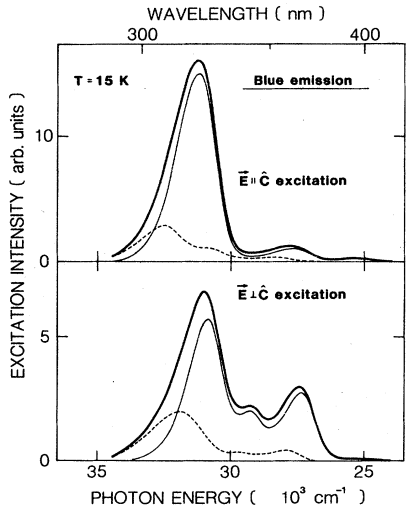

FIG. 6. Polarized excitation spectra for the blue emission at 15 K. The bold envelope is the measured excitation spectrum. The solid lines are excitation spectra for the slightly-polarized 450-nm emission and the dashed curves represent excitation spectra for the completely polarized 446.4-nm emission.

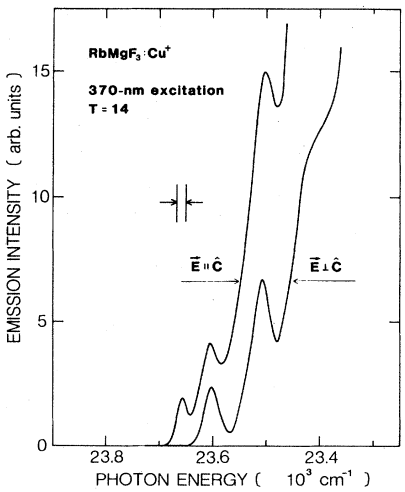

FIG. 8. Fine structure associated with the 450-nm emission for two different polarizations.

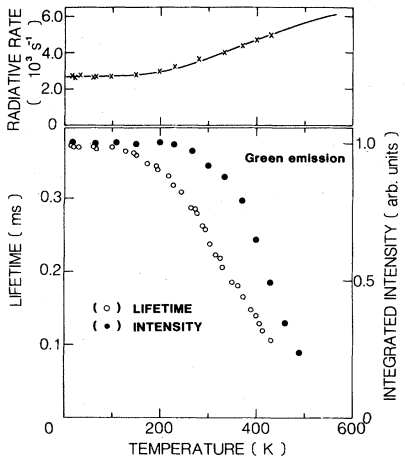

FIG. 9. Top, radiative transition rate ($\times$) as a function of temperature, obtained from the data shown in the bottom. The solid line is the best-fit curve of Eq. (3). Bottom, temperature dependence of the lifetime and the integrated intensity of the 575-nm emission.

tion of a higher level which is completely polarized $\mathbf{E}||\hat{c}$ and is responsible for the completely-polarized zero phonon line at 23 656 cm^{-1}.

As noted earlier the lifetime of the 450-nm emission at 14 K is 215 μs. It decreases rapidly with increasing temperature. If this lifetime quenching is due to thermalization, then it should be possible to fit the data using a three-level model consisting of two emission levels $|2\rangle$ and $|3\rangle$ and a ground state $|1\rangle$. For the model the decay rate of luminescence has, in general, two components given by

$$\tau=\tfrac{1}{2}\{(k_{21}+k_{31}+k_{23}+k_{32}) \pm[(k_{21}+k_{23}-k_{31}-k_{32})^2+4k_{23}k_{32}]^{1/2}\}\ , \quad (2)$$

where k_{ij} is a transition rate from $|i\rangle$ to $|j\rangle$.[21] Since no fast component of the 450-nm luminescence was observed within the time resolution (20 ns) of the detection system, the relaxation rates between the two upper levels are higher than the radiative rate between the levels and the ground state. The decay of the luminescence is then given by the slow component which can be approximated by

$$\tau_s=\frac{k_{31}+(g_2/g_3)k_{21}e^{-\Delta E/kT}}{1+(g_2/g_3)e^{-\Delta E/kT}}\ , \quad (3)$$

where g_2 and g_3 are the degeneracies of the two levels, and ΔE is the energy separation between the levels $|2\rangle$ and $|3\rangle$. The magnitude of ΔE in this case is 53 cm^{-1}. For several possible values of g_2/g_3, k_2 and k_3 were determined by fitting Eq. (3) to the experimental data. The best fit values of k_2 and k_3, for $g_2/g_3=2$, are 4.9×10^4 s^{-1} and 4.7×10^3 s^{-1}, respectively.

C. The 575-nm "green" emission

The temperature dependence of the lifetime and the integrated intensity of the 575-nm emission are depicted in the lower part of Fig. 9. The intensity is constant to 300 K, whereas the lifetime decreases around 100 K. This difference in temperature dependence suggests that two processes, thermalization and nonradiative transitions, are responsible for the decrease in lifetime. In this case, thermalization between energy levels occurs around 100 K and nonradiative decay is predominant above 300 K. A knowledge of both the lifetime and the relative quantum yield of luminescence, allows a determination of radiative and nonradiative transition rates. The calculated radiative rate is shown in the upper part of Fig. 9. The difference between the observed decay rate and the radiative rate yields the nonradiative rate at a given temperature. These are tabulated in Table I. A three-level model similar to that used in the preceding section for the 450-nm emission was applied to analyze the temperature-dependent radiative transition rate. For several possible values of g_2/g_3, Eq. (3) was evaluated with experimental data to find k_{21}, k_{31}, and ΔE. The best-fit values for $g_2/g_3=1$ are 2.3×10^4 s^{-1}, 2.7×10^3 s^{-1}, and $\Delta E=620$ cm^{-1}, respectively. The solid curve in Fig. 9 was obtained using these values. Even though the value of g_2/g_3 is not known exactly, it is clear that the splitting of the two luminescence levels for the 575-nm emission is larger than that for the 450-nm emission by a factor of 10. Measurements were made in an attempt to observe fine structure for the 575-nm band. But no such structure could be detected within the sensitivity of the detection system. This fact shows that the electron-lattice coupling is much stronger for the "575-nm center" than that for the "450-nm center." The integrated intensity of the 575-nm emission is quenched

TABLE I. Nonradiative transition rates (s^{-1}) at several temperatures for Cu^+ ions at site II in $RbMgF_3$. The rates are calculated from linear coupling theory and a second model taking into account quadratic coupling.

Temperature (K)	Experimental results	Linear coupling model	Linear and quadratic coupling model $\theta=44°$ $\hbar\omega=194$ cm^{-1}	$\theta=43°$ $\hbar\omega=170$ cm^{-1}	$\theta=42.5°$ $\hbar\omega=150$ cm^{-1}
25		2.2×10^{-20}	6.0×10^{-20}	2.3×10^{-19}	3.4×10^{-21}
200		8.5×10^{-15}	2.6×10^{-11}	1.1×10^{-7}	3.4×10^{-4}
300	3.2×10^2	5.2×10^{-11}	1.6×10^{-6}	6.7×10^{-3}	6.07×10^2
370	1.2×10^3	3.0×10^{-9}	5.8×10^{-4}	1.8	1.8×10^5
430	5.0×10^3	2.3×10^{-8}	1.4×10^{-2}	3.7×10^1	2.8×10^6
490	1.8×10^4	2.0×10^{-7}	4.5×10^{-1}	9.7×10^2	5.0×10^7

above 300 K (Fig. 9). This quenching temperature is much lower than that for the 450-nm emission (see Fig. 7) and the Cu^+ emission in other hosts. A detailed discussion of nonradiative multiphonon transitions will be presented in Sec. IV.

The peak energy of the 575-nm emission moves to high energy as the temperature increases (17 390 cm^{-1} at 14 K and 18 400 cm^{-1} at 400 K). The 450-nm emission peak shifts to lower energy. The latter behavior is expected from lattice dilation. The blue shift of the 575-nm emission can be partly attributed to the thermalization of the upper luminescent level which is situated 510 cm^{-1} above the lower level. The peak shift is, however, more than 1000 cm^{-1}, which is much greater than would result from a thermalization process. Such a shift can be explained by a strong nonlinear quadratic coupling between the Cu^+ electron and the lattice.

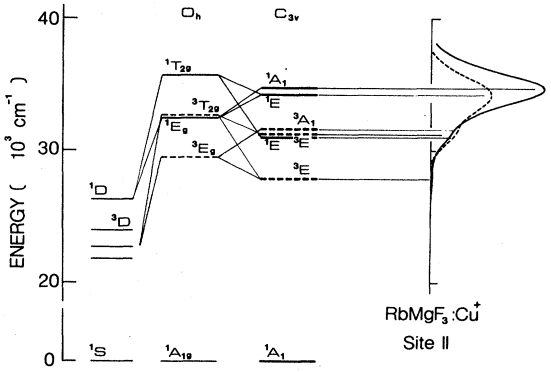

FIG. 11. Energy-level diagram of a Cu^+ ion situated in site II as illustrated in Fig. 10.

IV. DISCUSSION

A. Site assignments

The two Rb^+ sites in $RbMgF_3$ are shown schematically in Fig. 10. One site with D_{3h} symmetry (site I) has two Mg^{2+} ions at equidistant positions along the c axis, whereas the other (site II) has a Mg^{2+} ion and a Rb^+ ion as neighbors along the c axis. In site II the Rb^+ ion is further from the site center than the Mg^{2+} ion, thus a strong electrostatic field along the c axis is expected.

The spectral features of the "blue" and "green" bands are similar. Polarization measurements of emission and excitation spectra show that the principal axes of the two centers responsible for the emission are parallel to the c axis. The primary spectral difference between the two centers is the width of the emission and excitation bands. The width of the 575-nm emission and its excitation peaks are 1.6 times greater than those of the corresponding bands for the 450-nm emission. Furthermore, the Stokes shift of the 575-nm emission (10 200 cm^{-1}) is much larger than that (3000 cm^{-1}) of the 450-nm emission. These differences suggest that the electron-lattice coupling is strongest at the site responsible for the 575-nm emission. It is well known that electron-lattice coupling is greatest for systems in which the electron charge distribution changes greatly upon excitation.[22] In site II a strong electrostatic field exists along the c axis which will greatly change the charge distribution in the $(3d^9)(4s)\rightarrow(3d)^{10}$ transition. At site I no such polarization is expected. Thus, it is concluded that a Cu^+ ion at site II would experience strong electron-lattice coupling such as is evidenced by the width of 575-nm emission. The integrated intensity of the 575-nm emission is twice as great as the 450-nm emission. This suggests twice as many sites. Site II has twice as many sites as site I. Therefore, the data support the assignment of the 575-nm emission to Cu^+ ions in site II.

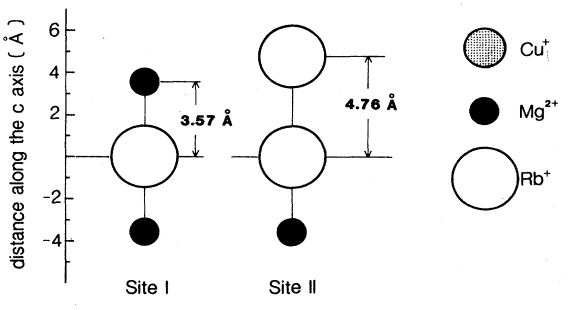

FIG. 10. Schematic diagram of the two Rb^+-ion lattice sites in $RbMgF_3$.

In Fig. 11 the energy-level diagram of a Cu^+ ion for site II with C_{3v} symmetry is depicted based on the experimental results for the 575-nm emission defect. This figure also includes the level diagram for a Cu^+ ion in NaF which has O_h symmetry.[15] The most intense band with totally symmetric (A_1) wave function occurs at the highest energy. The state is composed of a $4s$ electron and a hole in the $3d_{z^2}$ orbital. The corresponding state (E_g) in O_h symmetry has the lowest energy. The change in level ordering for a C_{3v} site may be ascribed to the stronger electrostatic repulsion between a hole at $3d_{z^2}$ orbital and neighboring cations situated along the c axis. Even though assignments of the other states in the excitation spectra are not straightforward, it appears the higher-E state is composed of $3d_{xy}$ and $3d_{x^2-y^2}$ orbitals and the lower one of $3d_{xy}$ and $3d_{yz}$ orbitals, respectively.

We now turn our attention to site I. A group-theory analysis for transitions of Cu^+ ions in D_{3h} symmetry such as in site I reveals that only one transition $(A_1\rightarrow E')$, the dipole moment of which is perpendicular to the c axis, is allowed for $3d^{10}\rightarrow 3d^9 4s$ transitions. The observed excitation spectrum for the 450-nm emission is not consistent with this prediction. One strong transition is excited with $\mathbf{E}\|\hat{\mathbf{c}}$ and two strong transitions occur from $\mathbf{E}\|\hat{\mathbf{c}}$ excitation (Fig. 2). These data are characteristic of Cu^+ ions in C_{3v} symmetry. Earlier experiments indicate that a small Cu^+ ion replacing a larger host cation tends to occupy an off-center site. Thus a Cu^+ ion at site I in $RbMgF_3$ crystals is most likely in an off-center configuration. In fact, it is likely that in $RbMgF_3$ several off-center sites exist around the Rb^+ location. The two different

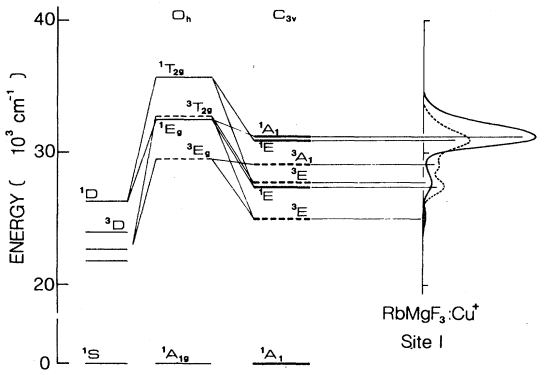

FIG. 12. Energy-level diagram of a Cu^+ ion situated in site I as illustrated in Fig. 10.

sets of emission and excitation spectra for the 450-nm emission at low temperature (<40 K) may correspond to different off-center configurations. The existence of off-center sites for the normally D_{3h} Rb^+ location changes the defect symmetry to C_{3v} through a displacement along the c axis. Figure 12 illustrates an energy-level diagram based on the data for site I. This diagram was formed by analyzing experimental data and taking into account the exchange energy, the magnitude of which is assumed to be the same as that for a Cu^+ ion in NaF, and the spin-orbit coupling. The success of describing the data, including the relative intensities of the excitation spectrum, increases confidence that Cu^+ ions at site I occupy off-center configuration along the c axis.

The energy-level diagram in Fig. 12 suggests that the 450-nm emission band is due to a transition between the lowest ^3E state and the A_1 ground state. Through spin-orbit coupling the ^3E state splits into A_1, A_2, and $2E$ levels. In the preceding section it was shown that two levels are involved in the emission process. The upper level, which is coupled to the ground state through an electric dipole moment parallel to the c axis, can be assigned to the A_1 level. But the lower level(s) cannot easily be assigned as E levels, since the experimental results indicate that the dipole moment of the transition from the lower level is almost isotropic, whereas the E levels are expected to have the dipole moments perpendicular to the c axis. An additional distortion of a Cu^+ ion within the plane perpendicular to the c axis, E-mode distortion, can explain the isotropic polarization of the emission from the lower states. Through this E-mode distortion, A_1 and E levels are mixed. Since the A_1 level has a higher radiative transition rate by a factor of 10 than the lower levels, a small amount of admixture (5%) is sufficient to make the polarization of the lower-level emission essentially unpolarized. The splitting of 53 cm^{-1} between the two excited-state levels, which is twice as large as for the Cu^+ ion in NaF,[16] may partly be due to this E-mode interaction. Such an E-mode distortion may be possible through either the dynamic Jahn-Teller effect or the mixed off-center configuration of the ground state.

B. Luminescence quenching of the 575-nm band

The luminescence intensity of the 450-nm emission is constant until 500 K, as is the case for Cu^+ luminescence in alkali halides.[1,12,14] It is unusual that the intensity of the 575-nm emission is quenched above 300 K, as seen in Fig. 9. As noted earlier, the site-II Cu^+ ions in $RbMgF_3$ show the strongest electron-lattice coupling of any host studied to date. Also, nonlinear coupling may be significant in this case. It is therefore of interest to examine the quenching mechanism of the 575-nm emission in terms of nonradiative transition theory with respect to electron-lattice coupling strength.

The nonradiative transition rate between two states, under usual approximations, is given by

$$k_{\mathrm{NR}}=\frac{2\pi}{\hbar}\,|M|^2G\ , \tag{4}$$

where M is a transition matrix element and G is the thermally averaged Franck-Condon factor evaluated under the energy-conservation condition.[22,23] In the framework of linear coupling, G is given by

$$G=\exp[-(2n+1)S](n+1/n)^{p/2}I_p[2Sn(n+1)]\ , \tag{5}$$

where S is the Huang-Rhys factor, n the phonon occupation number, p the integer given by the energy gap divided by the phonon energy, and I_p the modified Bessel function.[22] One dominant phonon mode is assumed in Eq. (5). In this model the magnitudes of S and $\hbar\omega$ can be evaluated from spectroscopic data. As seen in Fig. 2, the Stokes shift, given by $2S(\hbar\omega)$, is 10 150 cm^{-1}. On the other hand, the second moment of the emission band, given by $S(\hbar\omega)^2$ at low temperature, is 1 127 100 cm^{-2}. These two experimental values yield $S=24$ and $\hbar\omega=220$ cm^{-1} for the 575-nm emission. Using these values, and fixing the electronic part of Eq. (4) to 10^{13} s^{-1}, the magnitude of nonradiative transitions can be determined. The results for several temperatures are given in Table I, and compared with experimental results. It is clear that the predicted rate is too low over the whole temperature region. Thus the simple theory is inadequate to describe the observed rate.

It was suggested earlier that nonlinear electron-phonon coupling could be significant in the 575-nm emission. For nonradiative transitions, vibrational wave functions with higher quantum numbers at the ground state are mainly responsible for the Franck-Condon factor in Eq. (4). Those wave functions have greatest amplitude at the edge of the configuration coordinate parabola. Quadratic coupling broadens the vibrational wave functions of the initial state so that a great enhancement of the Franck-Condon factor results. Furthermore, the lower phonon energy allows a greater populate of the higher vibrational states and these have larger overlap integrals with the ground state. Thus, the quadratic coupling is expected to significantly enhance the nonradiative transition rate. The effect of the quadratic coupling on the nonradiative transition rate for the 575-nm emission, can be approximated by using the method formulated by Struck and Fonger.[23] Struck and Fonger have developed a method

for calculating the G factor in Eq. (5) for displaced and distorted potential curves. In this case the important quantities which determine the Franck-Condon factor are the ratio between the phonon energies of initial and final states of the transition, and the displacement of the coordinates of the minima of upper and lower potential curves. The former is characterized by a Mannebach angle θ, with $\tan^2\theta = (\hbar\omega_i/\hbar\omega_f)$ and ω_i and ω_f are phonon frequencies at initial and final states, respectively. The blue shift of the 575-nm emission band with temperature indicates that $\hbar\omega_i < \hbar\omega_f$, i.e., $\theta < 45°$.

According to the semiclassical treatment of the Franck-Condon principle, the width W_e of the emission band at lower temperatures is given by[21]

$$W_e^2 = 8\ln(2)\hbar\omega_f E_{LR}/\tan^2\theta(1+\tan^4\theta)\ , \tag{6}$$

where E_{LR} is the Stokes shift. The magnitude of $\hbar\omega_f$ and θ cannot be determined uniquely from the experimental values of E_{LR} and W_e. Instead, k_{NR} can be found for several possible cases of $\hbar\omega_f$ and θ. All quantities used in the calculation were determined so that E_{LR} is consistent with the experimental results.

The calculated results are listed in Table I. It can be seen that quadratic coupling enhances the rate of nonradiative transition significantly. A difference of 10% in phonon energies between initial and final states results in the enhancement of k_{NR} by 10^6. The calculated results shown above have only qualitative significance. However, it is clear that the quadratic coupling enhances the nonradiative transition rate significantly. Thus one may conclude that the quenching of the luminescence of the 575-nm emission at temperatures considerably lower than usual for Cu^+ ions is due to an enhanced nonradiative transition rate arising from nonlinear electron-lattice coupling. Recently Payne and McClure[24] have suggested that in the excited state Cu ions could form CuF molecules. If this occurs the Cu ions would be very strongly coupled to the lattice which could explain our observations.

V. SUMMARY

$RbMgF_3$ is an ideal host for investigating the optical properties of impurity ions such as Cu^+ in different site symmetries. The Rb^+ ions in this crystal reside in two different sites. When Cu^+ ions are substituted for Rb^+ ions two distinct emission bands at 450 and 575 nm are observed. Detailed optical measurements make it possible to produce energy-level diagrams, assign the sites responsible for the emission, and describe the low-temperature polarization effects. Specifically, it is shown that the small Cu^+ ions (radii 0.96 Å) when substituting for the larger Rb^+ ions (radii 1.47 Å) reside off center. Changes in the intensity and lifetime of the emission with temperature can be explained by thermalization of close energy levels and by nonradiative transitions.

ACKNOWLEDGMENTS

The authors wish to acknowledge the assistance of Mort Robinson of Hughes Research Laboratories, and M. D. Shinn, of Lawrence Livermore Laboratory. This work was done under National Science Foundation Grant No. DMR 84-06476.

[1]R. Oggioni and P. Scaramelli, Phys. Status Solidi **9**, 411 (1965).
[2]E. Krafzing, T. Timusk, and W. Martienssen, Phys. Status Solidi **10**, 709 (1965).
[3]K. Fassgaenger, Phys. Status Solidi **34**, 157 (1969).
[4]M. Piccirilli and G. Spinolo, Phys. Rev. B **4**, 1339 (1971).
[5]K. L. Yip and W. B. Fowler, Phys. Status Solidi B **53**, 137 (1972).
[6]H. S. Li, M. de Souza, and F. Lüty, Phys. Rev. B **7**, 4677 (1973).
[7]R. V. Jimenez and F. Lüty, Phys. Rev. B **12**, 1531 (1975).
[8]J. Simonetti and D. S. McClure, Phys. Rev. B **16**, 3887 (1977).
[9]C. Pedrini, Phys. Status Solidi B **87**, 273 (1978).
[10]V. Holland and F. Lüty, Phys. Rev. B **19**, 4298 (1979).
[11]T. Tsuboi, Phys. Rev. B **22**, 1871 (1980).
[12]C. Pedrini and B. Jacquier, J. Phys. C **13**, 4791 (1980); B. Moine and C. Pedrini, Phys. Rev. B **30**, 992 (1984).
[13]H. Chermette and C. Pedrini, J. Chem. Phys. **75**, 1869 (1981); **77**, 2460 (1982).
[14]A. B. Goldberg, D. S. McClure, and C. Pedrini, Chem. Phys. Lett. **87**, 508 (1982).
[15]S. A. Payne, A. B. Goldberg, and D. S. McClure, J. Chem. Phys. **78**, 3688 (1983).
[16]S. A. Payne, R. H. Austin, and D. S. McClure, Phys. Rev. B **29**, 32 (1984).
[17]L. DeShazer (unpublished).
[18]R. C. Pastor and M. Robinson, Mater. Res. Bull. **9**, 569 (1974).
[19]R. C. Pastor and A. C. Pastor, Mater. Res. Bull. **10**, 117 (1975).
[20]R. C. Pastor and K. Arita, Mater. Res. Bull. **10**, 493 (1975); **11**, 1037 (1976).
[21]See, for example, B. D. Bartolo, *Optical Interactions in Solids* (Wiley, New York, 1968).
[22]A. M. Stoneham, *Theory of Defects in Solids* (Clarendon, Oxford, 1975).
[23]C. W. Struck and W. H. Fonger, J. Lumin. **10**, 1 (1975); W. H. Fonger and C. W. Stuck, *ibid.* **17**, 241 (1978).
[24]S. A. Payne and D. S. McClure, J. Phys. Chem. **88**, 1379 (1984).